



Article

Preparation of Silicon Oxide-Carbon Composite with Tailored Electrochemical Properties for Anode in Lithium-Ion Batteries

Sang Jin Kim^{1,2,†}, Seung-Jae Ha^{1,3,†}, Jea Uk Lee², Young-Pyo Jeon^{1,3,*} and Jin-Yong Hong^{1,3,*} 

¹ C1 Gas & Carbon Convergent Research Center, Korea Research Institute of Chemical Technology, Daejeon 34114, Republic of Korea; pooh@kriect.re.kr (S.J.K.); smile@kriect.re.kr (S.-J.H.)

² Department of Advanced Materials Engineering for Information and Electronics, Integrated Education Institute for Frontier Science and Technology (BK21 Four), Kyung Hee University, 1732 Deogyong-daero, Giheung-gu, Yongin-si 17104, Republic of Korea; leejuk@khu.ac.kr

³ Advanced Materials and Chemical Engineering, University of Science and Technology (UST), Gajeong-ro, Yuseong-gu, Daejeon 34113, Republic of Korea

* Correspondence: ypjeon@kriect.re.kr (Y.-P.J.); jyhong@kriect.re.kr (J.-Y.H.);
Tel.: +82-42-860-7199 (Y.-P.J.); +82-42-860-7591 (J.-Y.H.)

† These authors contributed equally to this work.

Abstract: For high-efficiency and high-stability lithium ion batteries, a silicon oxide-based carbon composite has been developed as an anode material. To minimize structural defects (cracking and pulverization) due to volumetric contraction/expansion during charge/discharge, silicon oxide (SiO_x) is adopted. A pitch—a carbon precursor—is introduced to the surface of SiO_x using the mechanofusion method. The introduced pitch precursor can be readily transformed into a carbon layer through stabilization and carbonization processes, resulting in $\text{SiO}_x@\text{C}$. This carbon layer plays a crucial role in buffering the volume expansion of SiO_x during lithiation/delithiation processes, enhancing electrical conductivity, and preventing direct contact with the electrolyte. In order to improve the capacity and cycle stability of SiO_x , the electrochemical performances of $\text{SiO}_x@\text{C}$ composites are comparatively analyzed according to the mixing ratio of SiO_x and pitch, as well as the loading amount in the anode material. Compared to pristine SiO_x , the $\text{SiO}_x@\text{C}$ composite prepared through the optimization of the experimental conditions exhibits approximately 1.6 and 1.8 times higher discharge capacity and initial coulombic efficiency, respectively. In addition, it shows excellent capacity retention and cycle stability, even after more than 300 charge and discharge tests.

Keywords: silicon oxide; mechanofusion; carbon; composite; lithium ion batteries; anode



Citation: Kim, S.J.; Ha, S.-J.; Lee, J.U.; Jeon, Y.-P.; Hong, J.-Y. Preparation of Silicon Oxide-Carbon Composite with Tailored Electrochemical Properties for Anode in Lithium-Ion Batteries. *C* **2023**, *9*, 114. <https://doi.org/10.3390/c9040114>

Academic Editors: Jorge Bedia and Aleksey A. Vedyagin

Received: 5 October 2023

Revised: 13 November 2023

Accepted: 29 November 2023

Published: 1 December 2023



Copyright: © 2023 by the authors. Licensee MDPI, Basel, Switzerland. This article is an open access article distributed under the terms and conditions of the Creative Commons Attribution (CC BY) license (<https://creativecommons.org/licenses/by/4.0/>).

1. Introduction

At present, as the development and distribution of medium-to-large batteries for electric vehicles and energy storage increases, demand for lithium-ion battery (LIBs) market is also steadily increasing. In LIBs, the cathode material is responsible for energy generation, while the anode material functions in energy storage and release. The determination of the energy density hinges on the capacity to create substantial energy during the charging phase, a task predominantly governed by the cathode material. To date, extensive research efforts have predominantly concentrated on enhancing the cathode materials. However, the usefulness of the energy generated from the anode material depends on either adequate storage capacity or optimal exhaust efficiency. Therefore, for efficient energy storage, the importance of anode materials with high capacity and excellent stability is increasing.

The anode material of LIBs is mostly composed of natural or artificial graphite. However, artificial graphite anode materials have reached their theoretical capacity limit (372 mAh/g) and are limited in meeting the rising demands for high energy and power. Therefore, there is a need for the development of new materials to achieve high-capacity batteries [1–4].

Silicon (Si) offers a high theoretical capacity of around 4200 mAh/g, allowing it to store 15 lithium atoms (Li) per 4 Si atoms ($\text{Li}_{3.75}\text{Si}$), equivalent to 1 Li for every 6 carbon atoms (LiC_6) in comparison to carbon. However, the Si-based anodes experience significant volume expansion/contraction during charge/discharge cycles, leading to electrode pulverization, solid electrolyte interphase (SEI) destruction, and structural collapse, resulting in decreased cycle stability [5–8]. To overcome these limitations, Silicon oxide (SiO_x , $0 < x < 2$) has emerged as a promising candidate. While SiO_x electrodes show lower capacity compared to pure Si, the oxides (such as Li_2O and Li_4SiO_4) generated during charge/discharge function as a buffer against volume changes, leading to enhanced structural stability within the electrode. Additionally, SiO_x shows improved stability due to its lower reactivity with Li ions. These characteristics contribute to an excellent cycling performance and high energy density. However, the SiO_x still encounters challenges such as low initial efficiency, poor electrical conductivity, and significant volume changes during charge/discharge cycles [9]. Similar to the silicon, SiO_x also forms a passivation layer when it comes into direct contact with an electrolyte. This SEI layer can lead to a decrease in ionic conductivity and blockage of active sites, resulting in reduced initial Coulombic efficiency (ICE). Furthermore, the low electrical conductivity arising from the insulating properties of SiO_x can interrupt ion movement during the charging/discharging process, causing issues that deteriorate the electrochemical performance [10,11].

The most efficient way to solve these problems is to combine it with carbon materials or forming a carbon layer on the surface of SiO_x . By introducing the carbonaceous materials to the SiO_x , it becomes possible to suppress side reactions with the electrolyte and minimize the formation of a passivation layer, such as the SEI layer, which forms through irreversible reactions on the anode surface [12,13]. Furthermore, when using a carbon with excellent electrical conductivity and high thermal conductivity, not only can the charge transfer speed be enhanced, but also the thermal stability of the LIBs can be significantly improved [14].

Various research has reported coating or forming composites using carbon materials with Si and SiO_x [15–18]. It has been reported that Si/carbon composites can be produced through physical methods such as ball milling and spray drying technology [19]. In particular, Liu et al. manufactured spherical nanostructured Si/carbon composites using ball milling technology by employing nanometer-sized Si and fine graphite particles within a pyrolyzed carbon matrix [20]. As a chemical method, Yoshio et al. utilized a carbon precursor and thermal vapor deposition [21,22], while Kim et al. used pyrolysis fuel oil as a carbon precursor and utilized chemical vapor deposition for research aimed at introducing a carbon layer onto the surface of Si particles [23]. Additionally, Guo and his research team proposed a method for producing porous Si/carbon composites using a simple sol-gel method and a thermal imbalance reaction [24], and other studies utilizing various chemical methods have also been reported [25–27].

However, the previous research has primarily been conducted at the laboratory scale and faced limitations in terms of the manufacturing cost and yield from an industrial point of view. Therefore, for the practical mass production of high-capacity Si-based anode materials, it is essential to focus more on factors like ensuring capacity, improving the ICE, reducing manufacturing costs, and ensuring material mechanical safety.

Herein, a SiO_x -carbon ($\text{SiO}_x@\text{C}$) composite was produced using the simple mechanofusion method to address the challenges associated with Si as an anode material for LIBs. By using pitch with a high softening point as a carbon precursor, a stable carbon layer was formed on the SiO_x surface during the carbonization process. The optimal conditions for fabricating $\text{SiO}_x@\text{C}$ composites were established through the evaluation of the electrochemical properties of anode electrodes according to the mixing ratio of SiO_x and pitch, as well as the content ratio in the anode material. Additionally, the capacity retention and cycle stability were evaluated through cycle charge/discharge tests of the $\text{SiO}_x@\text{C}$ composite-based anode electrodes.

2. Materials and Methods

2.1. Materials

The graphite (MAGE, <25 μm , Hitachi, Tokyo, Japan) and SiO_x (DAEJOO electronic materials Co., Ltd., Siheung-si, Korea) were used as received. Pyrolysis fuel oil, which was supplied from Yecheon NCC (Yeosu, Korea) was used as the carbon precursor. The ash content of petroleum pitch confirmed 0.04 %, with 72.1% of fixed carbon. Carboxymethyl cellulose (CMC, Wellcos, Gunpo-si, Korea) and styrene-butadiene rubber (SBR, Wellcos, Gunpo-si, Korea) were used as binders; Super P (carbon black, Sigma-Aldrich, Burlington, MA, USA) was used as conducting additive; 1.0 M LiPF_6 in ethylene carbonate/diethylene carbonate (EC/DEC = 1:1 vol.%, Soulbrain, Seongnam-si, Korea), Celgard 2400 (Wellcos, Gunpo-si, Korea) was used as electrolytes and separators. All chemicals were used without further purification.

2.2. Fabrication of SiO_x @C Composites

The pitch was coated on the SiO_x using the mechanofusion method (NOB Nobilta mini, HOSOKAWA MICRON, Osaka, Japan). SiO_x and pitch were placed in the vessel and the mixing/dispersion process was performed through rotation of the equipment. In the mechanofusion process, the initial dry coating process was conducted at 2000 rpm for 20 min, followed by 4000 rpm for 10 min. After complexation, SiO_x -pitch composite was placed in the furnace. The stabilization processes were performed at 290 $^\circ\text{C}$ for 14 h with, a temperature increase rate of 5 $^\circ\text{C}/\text{h}$ in a nitrogen atmosphere. Then, carbonization was performed at 900 $^\circ\text{C}$ for 1 h with a temperature increase rate of 5 $^\circ\text{C}/\text{min}$. During the carbonization process, coking occurred from the carbon precursor on the surface of SiO_x . The prepared carbon-coated SiO_x samples were named SiO_x @C_9:1, SiO_x @C_8:2, SiO_x @C_7:3, and SiO_x @C_6:4 according to the different SiO_x /pitch weight ratios.

2.3. Fabrication of SiO_x @C Composite Anode Half Cell

For electrical characterizations, electrochemical tests were carried out using 2032 coin cells assembled using lithium metal foil as the counter electrode in an atmosphere of argon in a glove box. The electrodes were prepared from a coating slurry containing active materials, super-P, CMC, and SBR with a mass ratio of 95.5:1.1:1.1:2.3. The slurry was uniformly pasted on copper foils using a doctor blade and dried at 80 $^\circ\text{C}$ for 12 h in a vacuum oven. The diameter of the working electrodes was 14.0 mm, and the loading mass of the active materials was approximately 1.5 mg/cm^2 . The electrolyte was 1.0 M LiPF_6 dissolved in EC and DEC at a volume ratio of 1:1. Galvanostatic charge/discharge measurements were carried out in a voltage range of 0.01–1.5 V vs. Li/Li^+ at a current density of 40 mA/g for the first cycle. The assembled coin cells were evaluated with a multichannel battery cycler (WBCS3000, WonATech Co., Ltd., Seoul, Korea) to test their electrochemical performance. Charge/discharge tests were performed at a rate of 0.1 C within the cut-off voltage, ranging between 0.01 V and 2.0 V versus Li/Li^+ at room temperature. The rate characteristics were obtained by charging and discharging once at 0.1 C and then charging and discharging at different C-rates (0.2, 0.5, 1.0, 2.0 and 5.0 C) for 5 cycles each. The cycling stability was determined based on 100 cycles at a rate of 0.5 C.

2.4. Characterizations

Thermogravimetric analysis (TGA) of the prepared SiO_x @C composites was conducted using a SDT Q600 instrument (TA Instruments, New Castle, DE, USA). The morphologies and microstructures of the samples were characterized through Field-Emission scanning electron microscopy (FE-SEM) (JSM-6700F, JEOL, Tokyo, Japan), Energy-dispersive X-ray spectroscopy (EDS) (XFlash6, Bruker, Billerica, MA, USA), and transmission electron microscopy (TEM) (FEI, Tecnai G2-20, Hillsboro, OR, USA). $\text{Si}2p$ and $\text{C}1s$ binding energies of SiO_x @C composites were analyzed using X-ray Photoelectron Spectroscopy (XPS, KRATOS, AXIS Supra, Shimadzu, Kyoto, Japan). The BET analyses were performed using an ASAP 2020 (Micromeritics, Norcross, GA, USA) and using the N_2 adsorption-desorption

isotherms. Raman spectroscopy analyses (LabRAM HR-800, Horiba, Osaka, Japan) and powder electrical characteristics evaluation (HPRM-FA2, HANTECH, Gunpo-si, Korea) were carried out to investigate the chemical/mechanical properties of pristine SiO_x and the $\text{SiO}_x@\text{C}$ composites.

3. Results and Discussion

3.1. Mechanofusion-Derived $\text{SiO}_x@\text{C}$ Composites

The overall procedure for fabricating the $\text{SiO}_x@\text{C}$ composite using mechanofusion process is represented in Figure 1a. Mechanofusion is a method that efficiently combines different materials without the need for additional binders by applying three types of physical forces (compression, shear, and rotational forces) to internal particles [28]. The mechanofusion process is relatively simple, inexpensive, and requires no solvents, thereby making it potentially attractive for environmentally responsible commercial manufacture. Under our experiment condition, SiO_x served as the host material, while a pitch was used as the guest material to facilitate composite formation. Irregularly shaped SiO_x particles, averaging 1.8 μm in size, were used in the experiment. Furthermore, as a result of analyzing the oxidation level of pristine SiO_x through X-ray photoelectron spectroscopy (XPS) measurement, it was found that the x value of the SiO_x used in this work was 1.04 (see the Supplementary Materials Figure S1). The carbon precursor—the pitch—was prepared through the thermal polymerization of residual petroleum oil, which was previously reported in our work [29]. Due to the compression and shear forces generated between the blade and the rotating plate, independent SiO_x particles aggregate and combine with surrounding particles and pitch to form SiO_x -pitch composites ($\text{SiO}_x@\text{P}$). (Figure 1b). During this process, the high heat generated from the high-speed rotating plate, exceeding the softening point (S.P) of the pitch, increases the cohesion between the SiO_x particles and pitch by neither coating the SiO_x surface nor promoting particle–particle adhesion. Following complexation, the $\text{SiO}_x@\text{P}$ undergoes a transformation into a carbon layer through a stabilization and carbonization process. Generally, the thermoplastic feature of the pitch, the carbonization process, is performed after forming a crosslinking bond while undergoing a stabilization (insolubilization, oxidation) process at a temperature near the softening point to maintain the shape of the complex during the carbonization process [30]. The pitch used in this experiment had an S.P. of 270 $^\circ\text{C}$, and was stabilized at 290 $^\circ\text{C}$ for a sufficient period of time in an oxygen (O_2) atmosphere to form a more stable carbon structure. The carbonization yield of the coating pitch, as confirmed through the TGA curve, was 72% (see the Supplementary Materials Figure S2). Consequently, it is expected that pores will form inside the carbon layer after carbonization, and these pores are anticipated to facilitate the creation of a connection path for the electrolyte's active material and provide a buffering effect against volume expansion of SiO_x . A successful carbonization process was also visually confirmed by a color change in the sample. The initial dark brown SiO_x was transformed into black due to the presence of the carbon layer on the surface after composite formation and carbonization (Figure 1a inset).

3.2. Characterization of $\text{SiO}_x@\text{C}$ Composites

Changes in the particle size and shape resulting from the mechanofusion process were confirmed through SEM analysis. Figure 2a,b shows the particle shape before and after complexation, with the particle size analysis results shown in the inset. The pristine SiO_x particles showed a smooth surface with sharp edges, while the $\text{SiO}_x@\text{C}$ composites exhibited a rougher surface and blunt edges. This is because the surface becomes rougher as the coating pitch present on the composite surface goes through the stabilization/carbonization process. The particle analysis revealed that the D_{50} value of the pristine SiO_x was approximately 1.8 μm , whereas that of the $\text{SiO}_x@\text{C}$ composite was around 7.6 μm . These alterations in the surface morphology and particle size can be attributed to the composite formation process. During the mechanofusion process, a single SiO_x particle aggregates with

2–3 surrounding particles and the pitch, leading to an increase in the average particle size. This result is consistent with the complexation process mechanism described above.

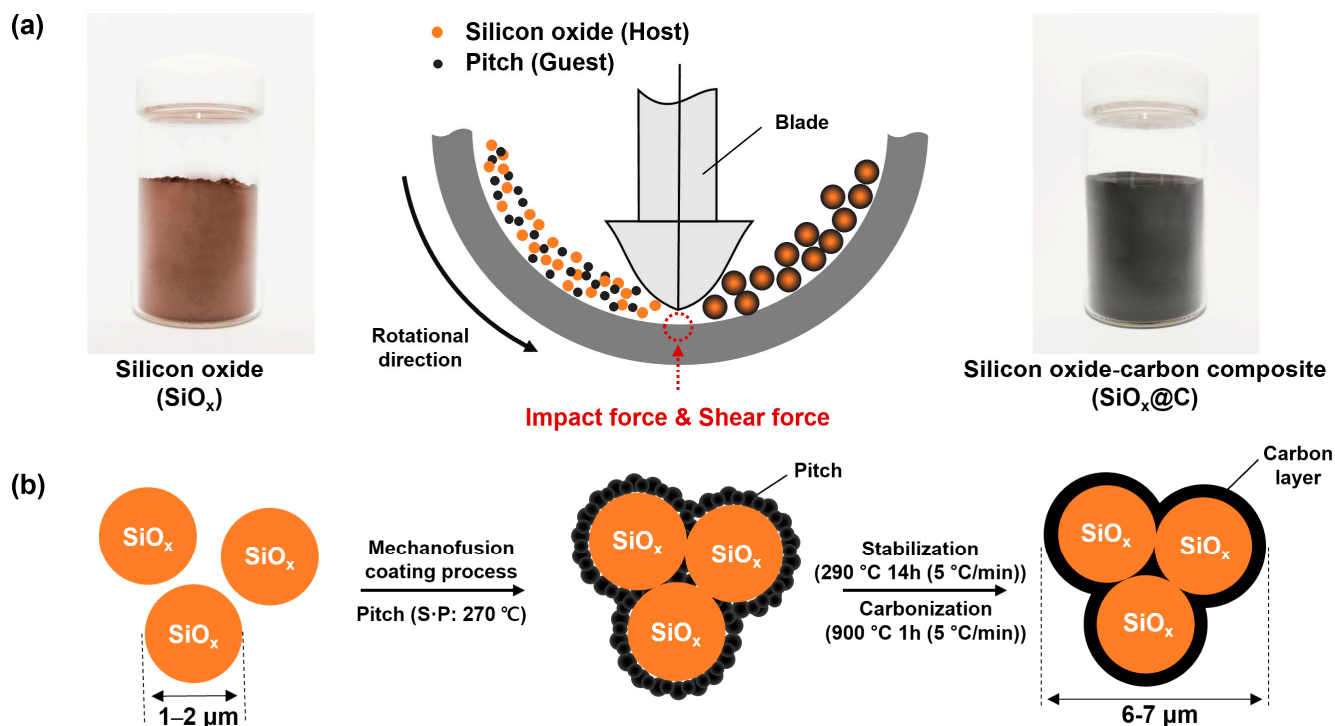


Figure 1. (a) Schematic illustration for fabricating $\text{SiO}_x@\text{C}$ composites by mechanofusion process, and digital photographs of SiO_x and $\text{SiO}_x@\text{C}$ composites. (b) Plausible schematic mechanism for the formation of $\text{SiO}_x@\text{C}$ composites.

Generally, it is known that the size of the anode active material should be 15 μm or less to provide a sufficient reaction surface area and maintain ionic/electronic conductivity during charging/discharging [31]. In the case of the $\text{SiO}_x@\text{C}$ composite prepared in this experiment, the average particle size is under 8 μm ; thus, it is considered that it may be applicable to the manufacturing process of an anode material without an additional particle sizing step.

EDS mapping analysis was also performed to confirm the formation of the carbon layer according to the stabilization and carbonization process. Figure 2c illustrates the SEM images of the $\text{SiO}_x@\text{C}$ composites along with the EDS mapping results. The elemental distribution analysis revealed the presence of silicon (76.9%), carbon (15.3%), and oxygen (7.6%) elements. It clearly shows that carbon elements are widely distributed throughout the whole $\text{SiO}_x@\text{C}$ composite surface, indicating the uniform formation of the carbon layer.

The carbon layer on the surface of the $\text{SiO}_x@\text{C}$ composites functions as a buffer layer, effectively minimizing structural defects such as cracks and pulverization caused by the volume expansion and contraction of SiO_x during charging/discharging. Additionally, it reduces contact resistance between active materials, facilitating rapid electron movement and providing an efficient pathway for electrons. The thickness of the carbon layer directly influences the electrochemical properties of the $\text{SiO}_x@\text{C}$ composites as it is closely related to the battery performance. Therefore, this study focuses on investigating the relation between the carbon layer thickness and the electrochemical properties by varying the amount of pitch during the fabrication of the $\text{SiO}_x@\text{C}$ composites via the mechanofusion method.

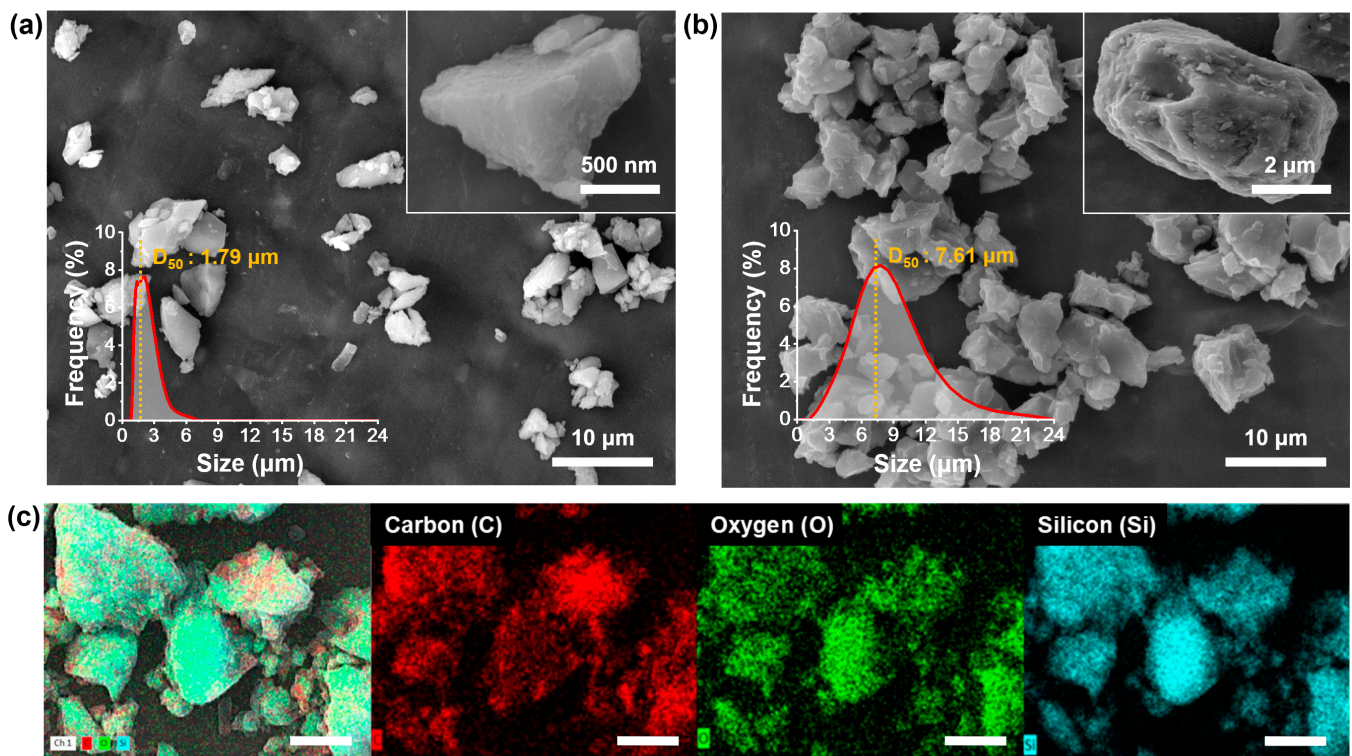


Figure 2. FE-SEM images and particle-size distribution of the (a) SiO_x and (b) $\text{SiO}_x@\text{C}$ composites (inset: SEM image of the corresponding sample with high magnification). (c) Energy dispersive X-ray spectroscopy (EDS) elemental maps of corresponding C, O, and Si in the $\text{SiO}_x@\text{C}$ composites (inset scale bar is 5 μm).

Changes in the carbon layer thickness of the $\text{SiO}_x@\text{C}$ composites were analyzed using TEM in response to variations in the pitch content for complexation. Figure 3a depicts the pristine SiO_x surface without the addition of the pitch. Figure 3b–e shows images of the $\text{SiO}_x@\text{C}$ composite surfaces with 10, 20, 30, and 40 wt% of pitch added compared to SiO_x , respectively. The pristine SiO_x shows a clean and smooth surface, whereas an increase in the coating pitch content leads to the roughening of the $\text{SiO}_x@\text{C}$ composite surface due to the influence of the formed carbon layer. Additionally, with the increase in pitch content, the amount of carbon precursor capable of binding to the SiO_x surface during the mechanofusion process also increased. This led to the gradual thickening of the carbon layer on the SiO_x surface, forming an amorphous carbon layer through stabilization and carbonization. Notably, the sample with 40 wt% added pitch ($\text{SiO}_x@\text{C}_{6:4}$) exhibited a carbon layer thickness of around 400 nm.

Figure 3f shows the correlation between the mixing ratio and coating layer thickness. The theoretical value was calculated based on the particle size analysis results, assuming a SiO_x radius of 3.8 μm , and the actual measured value was obtained from the TEM analysis results. Both the theoretical and actual values indicated that as the amount of added pitch increased, the carbon layer thickness also tended to increase. However, it was observed that the actual thickness of the carbon layer was slightly lower than the theoretical value. This discrepancy can be attributed to factors such as the irregularity of the SiO_x particle shape and incomplete composite formation. In the case of the pristine SiO_x , which possesses an irregular morphology rather than spherical shape, it is anticipated that the carbon layer thickness might be uneven. Additionally, the difference between the theoretical and measured values is likely due to the influence of residual pitch that did not participate in the mechanofusion process, resulting in incomplete composite formation.

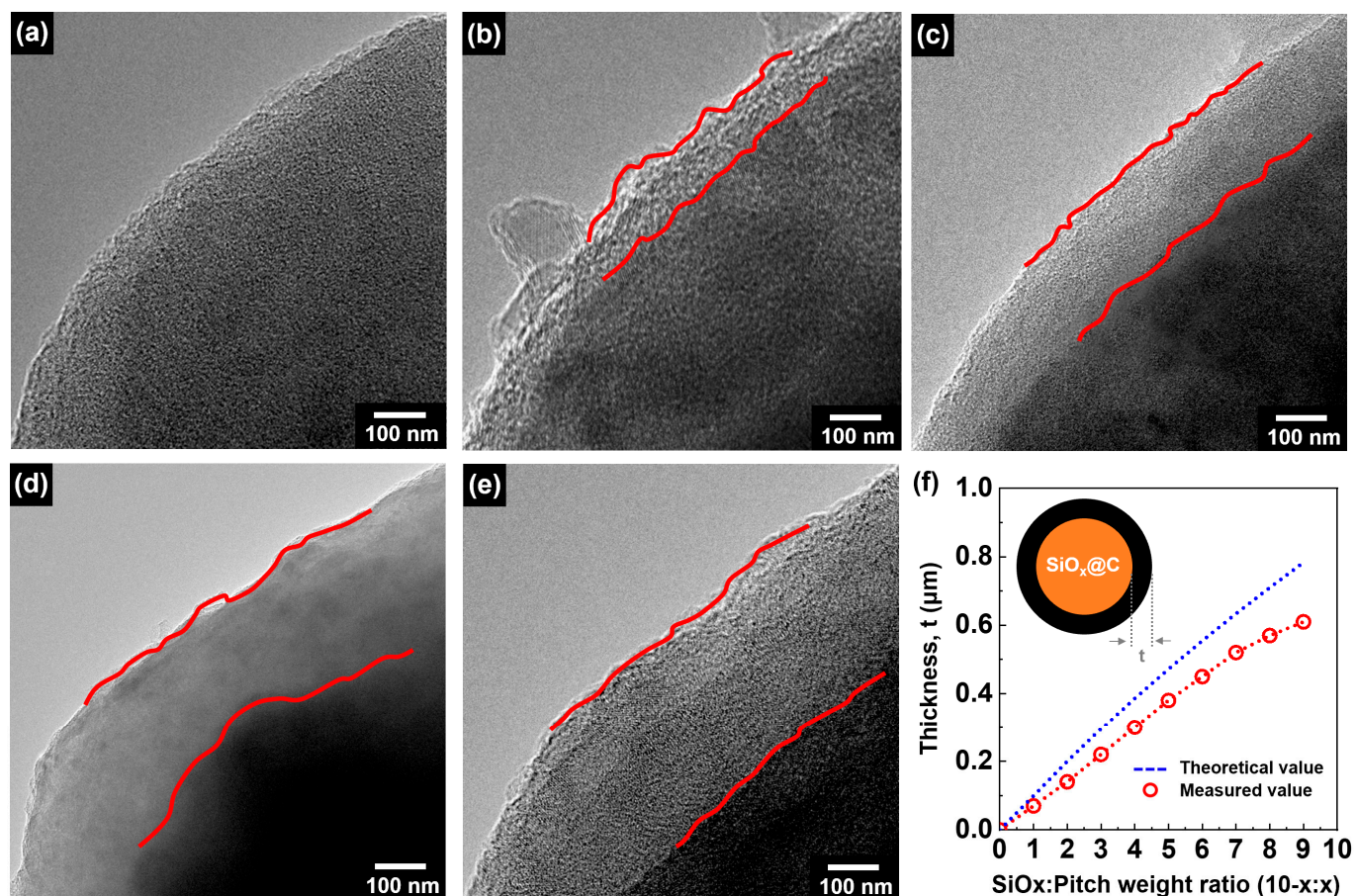


Figure 3. TEM images of the SiO_x@C composites prepared with different SiO_x/pitch weight ratios of (a) 0, (b) 10, (c) 20, (d) 30 and (e) 40. (f) Carbon layer thickness as a function of SiO_x/pitch weight ratios. Blue dot line and red circle indicate the theoretical and measured value, respectively.

The degree of structural defects in the carbon layer on the SiO_x surface was determined through Raman analysis, and the results are presented in Figure 4a. Both the pristine SiO_x and SiO_x@C composites show a peak at around 520 cm⁻¹, corresponding to the Si bulk single crystal, while the SiO_x@C composite displays carbon-related peaks at 1350 cm⁻¹ and 1600 cm⁻¹, corresponding to the D-band and G-band, respectively. The D-band indicates the degree of surface defect or disorder in the carbon layer, while the G-band represents unique characteristics related to the graphitization of the carbon layer [32].

In general, the relative intensity of the D-band to the G-band (I_D/I_G) serves as an indicator of the degree of defects in the carbon bond structure. A decrease in the I_D/I_G value means reduced defectiveness or increased crystallinity of the carbon bonding structure, while an increase in the I_D/I_G value indicates increased defectiveness or decreased crystallinity [33]. For the SiO_x@C composites, the I_D/I_G value was approximately 0.98, which was similar to the characteristic value of typical amorphous carbon. These results confirmed that the pitch composited with SiO_x particles was changed into an amorphous carbon layer, characterized by a mixed structure of sp² and sp³ bonds, through the stabilization and carbonization process. In addition, the sp²/sp³ bonding ratio of the carbon layer in the SiO_x@C composite was also investigated (see the Supplementary Materials Figure S3). From the C1s XPS peak, it is obvious that the carbon layer in the SiO_x@C composite exists in the sp² configuration more than the sp³ configuration, and it is revealed that the sp²/sp³ ratio is about 2.26. Consequently, it was verified that the pitch with a low content of volatile hydrocarbons can serve as an effective precursor for forming a carbon layer due to its high coking value.

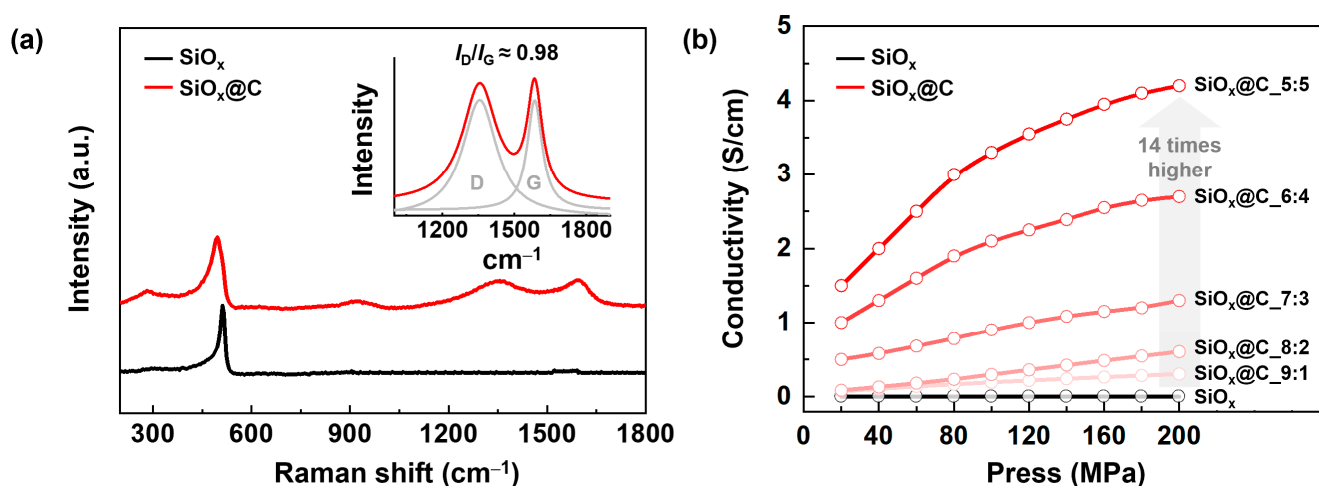


Figure 4. (a) Raman spectra of SiO_x and $\text{SiO}_x@\text{C}$ composite. (inset: Deconvoluted peaks on D and G band are indicated by a gray line). (b) Powder conductivity of $\text{SiO}_x@\text{C}$ composites prepared with different $\text{SiO}_x/\text{Pitch}$ weight ratios of 0, 10, 20, 30, 40 and 50 wt%.

The carbon layer introduced into SiO_x is anticipated to improve the electrical conductivity of SiO_x . Changes in the electrical properties of the $\text{SiO}_x@\text{C}$ composites prepared with varying amounts of pitch were analyzed using a powder resistance measurement (Figure 4b). The SiO_x is a representative insulating material known for its high dielectric breakdown strength and low leakage current. As a result, the SiO_x exhibited insulating properties, with electrical conductivity converging to 0 S/cm. In contrast, the $\text{SiO}_x@\text{C}$ composites showed an enhancement in electrical conductivity with the increasing content of added coating pitch. It was also confirmed that as the pitch content increases, the powder conductivity also increases faster at the same pressure. These phenomena are ascribed to the increased thickness of the carbon layer, which possesses excellent electrical conductivity. As the thickness of the carbon layer increases during the densification process under pressure, the reduction in the resistance per unit volume occurs due to the establishment of extended conductive channels. Under our experimental condition, the composite with 50 wt% added pitch ($\text{SiO}_x@\text{C}_5:5$) demonstrated superior electrical conductivity of 4.2 S/cm under a pressure of 200 MPa. This value is more than 14 times higher than that of the $\text{SiO}_x@\text{C}_9:1$ sample measured under the same conditions.

An electrochemical impedance spectroscopy (EIS) analysis was also performed for investigating the impedance of the cell containing $\text{SiO}_x@\text{C}$ composites (see the Supplementary Materials Figure S4). All $\text{SiO}_x@\text{C}$ composite cells have a lower charge transfer resistance (R_{ct}) than that of the SiO_x cells, and the R_{ct} value of the $\text{SiO}_x@\text{C}$ composites decreased with the increasing content of added coating pitch; this means that it has a smaller contact resistance and higher electrical conductivity as the thickness of the carbon layer increases. The R_{ct} value of the $\text{SiO}_x@\text{C}_6:4$ composite electrode is approximately 201 Ω , which is significantly lower than the R_{ct} of 372 Ω of the pristine SiO_x electrode.

The specific surface area of the anode material plays a crucial role in the initial charging and discharging processes of LIBs. The increased specific surface area of the active material provides advantages in terms of the capacity and rate characteristics. However, an excessive surface area can lead to the formation of irreversible compounds, such as SEI layers and $\text{Li}_2\text{Si}_2\text{O}_5$, Li_2SiO_3 , Li_4SiO_4 , resulting in reduced initial efficiency [34].

To examine the changes in the specific surface area and pore structure of the $\text{SiO}_x@\text{C}$ composite resulting from the carbon layer formation, nitrogen gas adsorption-desorption isotherms were conducted. As shown in Figure 5a, both the SiO_x and $\text{SiO}_x@\text{C}$ composites show similar adsorption isotherms, with minimal nitrogen adsorption at low relative pressures ($P/P_0 < 0.3$), suggesting the development of mesopores and macropores rather than micropores. For the specific surface area (S_{BET}), pristine SiO_x was determined to have

a value of $9.1 \text{ m}^2/\text{g}$. However, the S_{BET} of the $\text{SiO}_x@\text{C}$ composite ($\text{SiO}_x@\text{C}_{8:2}$) was about $6.0 \text{ m}^2/\text{g}$, which represents a relatively reduced value compared to the pristine SiO_x . This reduction is attributed to the increase in the average particle size resulting from particle agglomeration during the mechanofusion process.

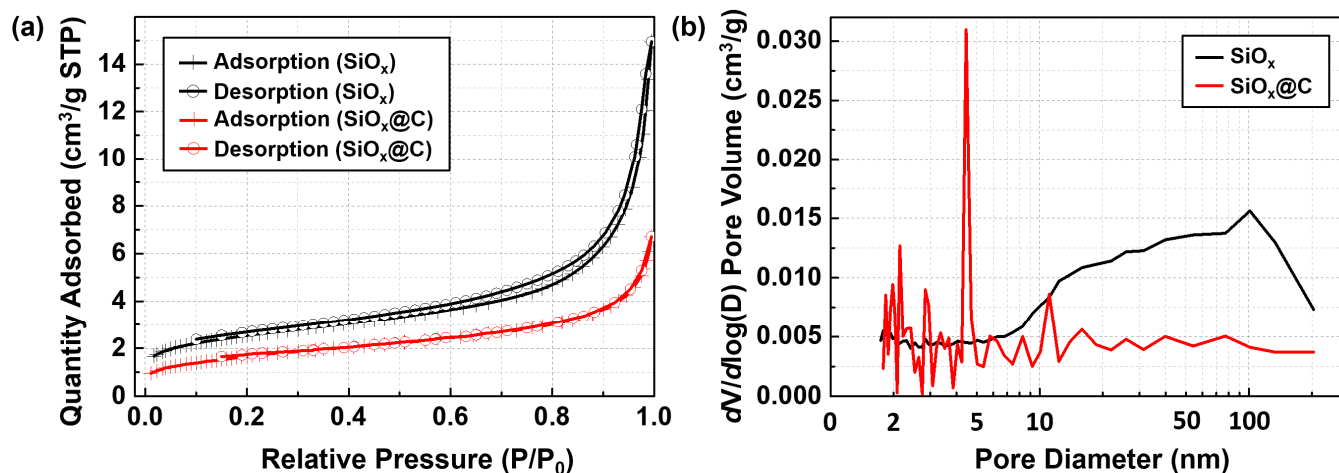


Figure 5. (a) Nitrogen adsorption–desorption isotherms and corresponding (b) BJH pore size distributions of the SiO_x and $\text{SiO}_x@\text{C}_{8:2}$ composites derived from desorption isotherms.

Generally, the specific surface area of electrode materials is considered suitable below $10 \text{ m}^2/\text{g}$, as larger values can negatively impact the battery life cycle [35]. The S_{BET} values of the $\text{SiO}_x@\text{C}$ composites prepared in this experiment ranged between 5 and $7 \text{ m}^2/\text{g}$, with no additional increase in the specific surface area observed through the mechanofusion composite process (Table 1). Under our experimental condition, the pore size was calculated from the desorption isotherm using the BJH (Barrett-Joyner-Halenda) method. As a result of the BJH pore size distribution analysis (Figure 5b), it can be seen that there are many pores with a diameter of 10 nm or more in the pristine SiO_x sample. On the other hand, in the case of the $\text{SiO}_x@\text{C}$ composite, most pores were found to be concentratedly distributed in the range of 0.9 to 10 nm, with an average size of 8.68 nm. Interestingly, following the mechanofusion process, there was a slight decrease in the S_{BET} value, while the pore volume increased by over 450%. This phenomenon can be explained by the development of micro- and meso-pores as a result of carbon layer formation. During the carbonization process, the stabilized pitch introduces reactions that involve the removal of oxygen and hydrogen functional groups, promoting the development of micro- and meso-pores on the surface. As a result, it was found that in the case of the $\text{SiO}_x@\text{C}$ composite, the microporosity and mesoporosity increased by 2.8% and 8.4%, respectively, while the macroporosity decreased to about 11.2% compared to the pristine SiO_x . Furthermore, the average pore size reduced by approximately 40% after the mechanofusion process (from 14.7 nm to 8.7 nm), indicating the development of smaller pores around the range of 2–10 nm. This observation coincides with the aforementioned increase in the mesopore volume and supports the explanation for the increase in the pore volume.

3.3. Battery Performance Evaluation of $\text{SiO}_x@\text{C}$ Composite Anode

The electrochemical properties of the anode materials were evaluated under various fabricating conditions and active material composition ratios, with all the charge/discharge curves presented in Figure 6a. The corresponding results for the discharge capacity and initial efficiency are summarized in Figure 6b,c, respectively.

Table 1. Summary of the porosity parameters of the SiO_x and $\text{SiO}_x@\text{C}$ _8:2 composites.

Sample	SiO_x	$\text{SiO}_x@\text{C}$ Composite
$S_{\text{BET}}^{(1)}$ (m^2/g)	9.06	6.00
$V_{\text{total}}^{(2)}$ (cm^3/g)	0.021	0.096
Micropore volume fraction (%)	1.6	4.4
Mesopore volume fraction (%)	50.9	59.3
Macropore volume fraction (%)	47.5	36.3
Average pore size (nm) ⁽³⁾	14.7	8.68

⁽¹⁾ Calculated from the BET surface area analysis. ⁽²⁾ The total pore volume was calculated at a relative pressure of 0.30. ⁽³⁾ The pore size was calculated from the desorption isotherm using the BJH method.

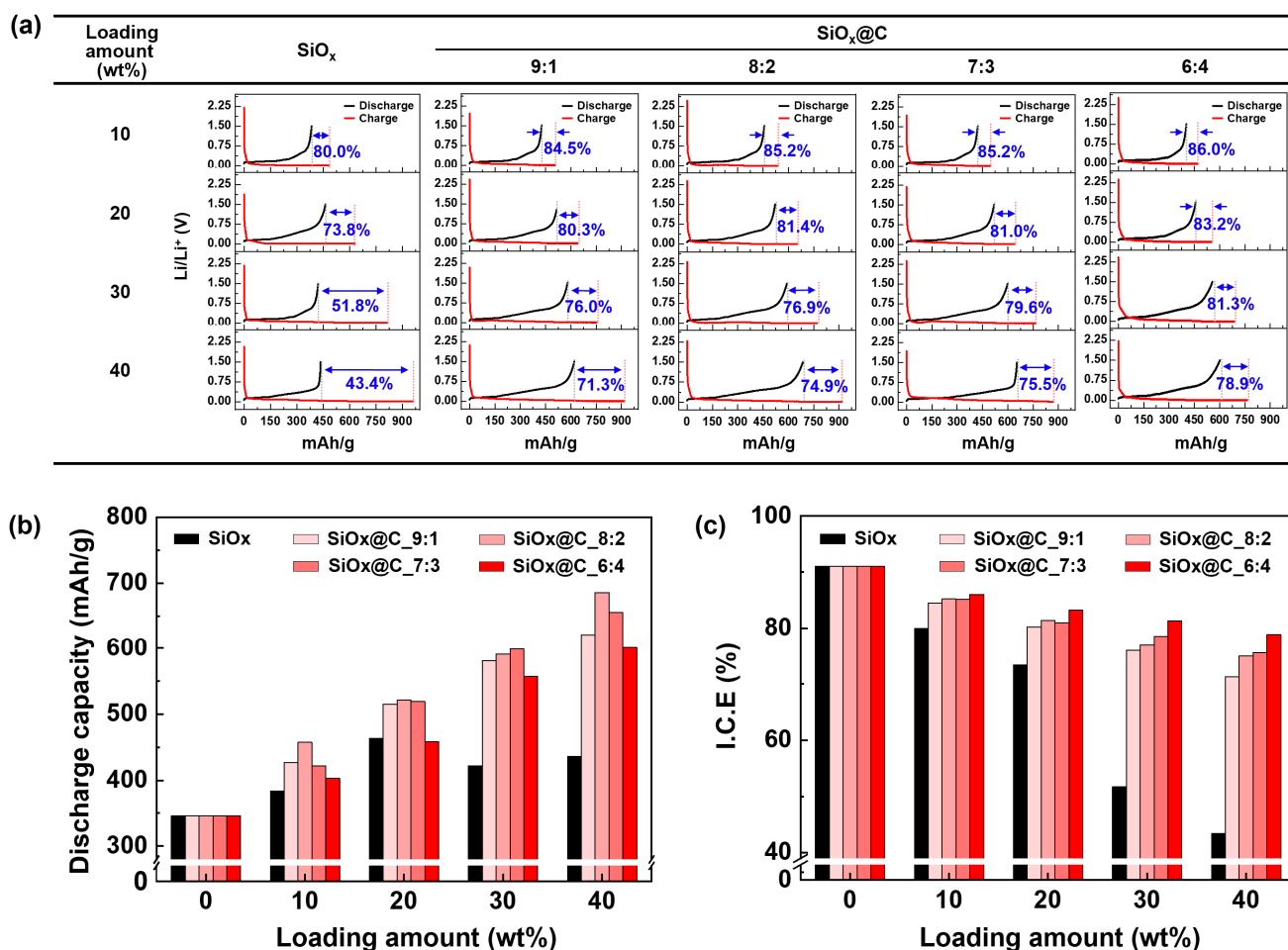


Figure 6. (a) The first charge/discharge voltage profiles of the anode using pristine SiO_x and $\text{SiO}_x@\text{C}$ composites prepared with the SiO_x /Pitch weight ratio of 0, 10, 20, 30, and 40. (b) Discharge capacity and (c) ICE as a function of loading amount (0–40 wt%). All cell tests were performed in a climate chamber at 25 °C with the rate of 0.2 C.

In the case of the anode electrode using only artificial graphite (AG) as the active material, a discharge capacity of 345.0 mAh/g and an initial efficiency of 91.0% were observed. This was comparable to the theoretical values of the typical AG-based anode materials (Figure 6b). In the case of the electrode prepared by adding pristine SiO_x to the AG, the discharge capacity was found to increase to 463.3 mAh/g, up to a loading amount of 20 wt%, after which it began to decrease. This decrease was attributed to the volume expansion of SiO_x during lithium intercalation, leading to pulverization and loss of electrical contact due to the resulting structural transformation [36].

For the $\text{SiO}_x@\text{C}$ composites, the carbon layer on the SiO_x surface effectively alleviated the volume expansion of SiO_x caused by lithiation/delithiation and maintained the electrical conductivity, resulting in an increase in the discharge capacity with the increasing loading amount. Although a consistent causal relationship between the mixing ratio and discharge capacity was not observed at the same loading amount, as the content of pitch increased, the discharge capacity tended to decrease. Namely, the carbon layer thickness of the $\text{SiO}_x@\text{C}$ composite and the discharge capacity showed an inverse relationship. This is attributed to SiO_x being the primary determinant of the discharge capacity in the $\text{SiO}_x@\text{C}$ composites. Unlike graphite, which stores lithium ions through an intercalation reaction within the graphitic layers, an amorphous carbon is known to have a small contribution to securing the discharge capacity. To confirm the capacity contribution of the carbon layer in the $\text{SiO}_x@\text{C}$ composite, the control experiments were carried out using carbonized pitch as a comparison material (see the Supplementary Materials Figure S5). The carbonized pitch is expected to have a capacity of approximately 25 mAh/g, and the carbon layer of the $\text{SiO}_x@\text{C}$ composite is believed to not contribute significantly to the capacity. The amorphous carbon layer introduced on the SiO_x surface only stored lithium ions in localized vacancies created by the unstable stacking structure of the carbon layer [37]. Otherwise, when the pitch content was low (e.g., $\text{SiO}_x@\text{C}_9:1$), the capacity retention was relatively reduced due to the decreased role of the carbon layer described earlier. The sample with the highest discharge capacity was the $\text{SiO}_x@\text{C}_8:2$ composite with the loading amount of 40 wt%. This sample showed a discharge capacity of 685 mAh/g, which was approximately 1.57 times higher than that of the pristine SiO_x at the same loading amount. The detailed charge storage mechanism according to the lithiation/delithiation process of the $\text{SiO}_x@\text{C}$ composite is shown in Supplementary Materials Figure S6.

Figure 6c represents the ICE of the samples prepared with different mixing ratios and active material compositions. Both the SiO_x and $\text{SiO}_x@\text{C}$ composites showed a tendency for the ICE value to decrease as the loading amount increased. In the case of the pristine SiO_x , the ICE value significantly decreased, reaching the lowest value of 43.4% when the loading amount was 40%. However, the $\text{SiO}_x@\text{C}$ composites showed relatively high ICE values. At the 40 wt% loading amount, the $\text{SiO}_x@\text{C}_6:4$ composites demonstrated an ICE of 78.9%. This value was approximately 1.82 times higher than that of pristine SiO_x . This improvement was attributed to the effective suppression of irreversible reactions and SEI formation by the carbon layer introduced on the SiO_x surface. At the same loading amount, it was observed that the ICE tends to increase with the higher pitch content for fabricating $\text{SiO}_x@\text{C}$ composites. In other words, an increased thickness of the carbon layer contributed to the enhanced stability of the active material. A thicker carbon layer introduced into the $\text{SiO}_x@\text{C}$ composites is more advantageous in terms of the ICE value, but less advantageous in terms of securing the discharge capacity. Therefore, in this study, based on the various cell test results, the $\text{SiO}_x@\text{C}_8:2$ composite sample was selected as the optimal mixing ratio for the anode material, and cycle stability tests were conducted.

Cycling measurements were conducted on the anodes consisting of the pristine SiO_x and $\text{SiO}_x@\text{C}_8:2$ composites at a current density of 1.0 C for the initial two cycles, and 0.5 C for the subsequent cycles. A compilation of investigations carried out using various $\text{SiO}_x@\text{carbon}$ composites is also presented in Supplementary Materials Figure S7. As depicted in Figure 7a, the $\text{SiO}_x@\text{C}_8:2$ composite shows a higher reversible capacity and more stable cycling performance compared to the pristine SiO_x . The anode containing the $\text{SiO}_x@\text{C}_8:2$ composite with the 20 wt% loading amount maintains about 60% of its initial charge capacity after 300 cycles, whereas the pristine SiO_x anode exhibits a significant decrease in capacity with a capacity retention rate of only 12.6% at 100 cycles.

Furthermore, the Coulombic efficiency of the SiO_x anode reaches 99% after 10 cycles, while the Coulombic efficiency of the $\text{SiO}_x@\text{C}_8:2$ anode achieves 99% after only 4 cycles (Figure 7b). The delayed attainment of 99% Coulombic efficiency in the SiO_x anode suggests the continued formation of SEI and excessive side reactions on untreated surfaces, potentially leading to a substantial capacity reduction by consuming limited Li^+ ions.

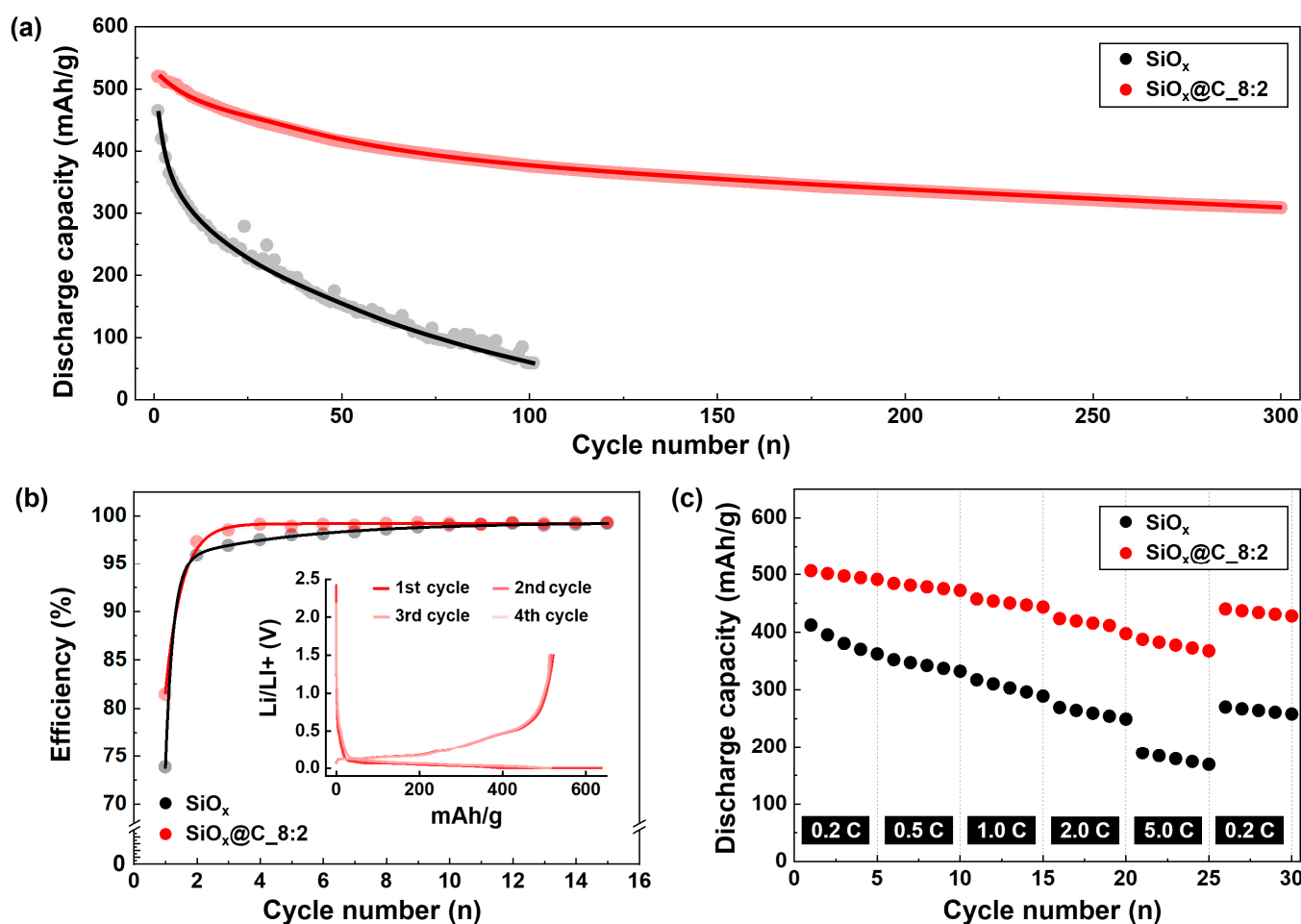


Figure 7. (a) Cycling performance and (b) current efficiency of the SiO_x and SiO_x@C_{8:2} composite at 0.5 C. (c) Rate capability at 0.2, 0.5, 1.0, 2.0, and 5.0 C for SiO_x and SiO_x@C_{8:2} composite at 25 °C.

Additionally, to compare the rate characteristics of the anode, the C-rate was measured at a current density of 0.1 C during the first cycle, followed by measurements at 0.2 C, 0.5 C, 1.0 C, 2.0 C, and 5.0 C for the subsequent five cycles (Figure 7c). In particular, the SiO_x@C_{8:2} composite demonstrated a stable specific capacity of 77.2% at a current density of 5.0 C compared to 0.2 C. Furthermore, as the current density was reduced from 5.0 C back to 0.2 C, the specific capacity recovered to 440 mAh/g. In contrast, the SiO_x anode showed relatively inferior rate characteristics, exhibiting a specific capacity of only 47.8% at a current density of 5.0 C compared to the established 0.2 C rate. Upon returning the current density from 5.0 C to 0.2 C, the SiO_x anode showed a specific capacity of only 189 mAh/g. Thus, it is believed that the carbon layer on the SiO_x@C composite induces the uniform formation of the SEI layer, thereby having a positive effect on battery cycle stability.

4. Conclusions

In summary, to overcome the inherent limitations of existing Si-based anode materials, the SiO_x-based carbon composite material was developed and applied as an anode material. Mechanofusion complexation was performed using the SiO_x and pitch as host and guest materials, respectively. During the mechanofusion process, the SiO_x particles aggregated and formed complexes with the surrounding particles and coating pitch, resulting in an increase in the average particle diameter from 1.8 μm to 6.7 μm. The introduced pitch was converted into a carbon layer through stabilization and carbonization processes, forming a uniform coating on the SiO_x surface, as confirmed by the EDS mapping analysis. The TEM analysis showed that as the pitch content increased, the carbon layer thickness also

increased, and this thickness could be adjusted from 0 to 600 nm by varying the pitch contents. The Raman analysis revealed a non-crystalline carbon layer with a mixture of sp^2 and sp^3 hybridized structures, while the BET analysis indicated the development of fine and mesopores within the carbon layer. The increased carbon layer thickness resulted in improved electrical conductivity, addressing the electrically insulating characteristic of pristine SiO_x . Based on the outstanding mechanical and excellent electrical properties of the carbon layer, the $SiO_x@C$ composites presented an enhanced discharge capacity and initial efficiency compared to the pristine SiO_x . The evaluation of the battery anode performance of the $SiO_x@C$ composites, considering the mixing ratio of silicon oxide and pitch, as well as the loading amount in the anode material, revealed that as the pitch content for the coating increased (resulting in thicker carbon layer), there was a decrease in the discharge capacity, but an increase in the initial efficiency. Notably, the $SiO_x@C_{8:2}$ composite material, produced through optimization, demonstrated a discharge capacity approximately 1.6 times higher and an initial efficiency approximately 1.8 times better at the same content level as the pristine SiO_x , maintaining excellent cycle stability for more than 300 cycles after the second cycle.

Supplementary Materials: The following supporting information can be downloaded at: <https://www.mdpi.com/article/10.3390/c9040114/s1>, S1: Oxidation level of pristine SiO_x ; S2: TGA analysis of pitch; S3: sp^2/sp^3 carbon ratio in $SiO_x@C$ composite; S4: EIS analysis; S5: Discharge capacity of carbon layer; S6: Charge storage mechanism; S7: Compilation of different investigations using various silicon oxide-carbon composites.

Author Contributions: Conceptualization, Y.-P.J. and J.-Y.H.; methodology, J.U.L.; validation, Y.-P.J. and J.-Y.H.; formal analysis, J.-Y.H.; investigation, S.J.K. and S.-J.H.; data curation, J.-Y.H., S.-J.H. and J.U.L.; writing—original draft preparation, S.J.K.; writing—review and editing, Y.-P.J. and J.-Y.H. All authors have read and agreed to the published version of the manuscript.

Funding: This work was supported by the Technology Innovation Program (20006777, 20006778), by the Industrial Strategic Technology Development Program (20012763), and by the Energy Core Technology Program (1415186918) funded by the Ministry of Trade, Industry and Energy (MOTIE, Korea). The APC was funded by the Industrial Strategic Technology Development Program.

Data Availability Statement: Data are contained within the article and supplementary materials.

Conflicts of Interest: The authors declare no conflict of interest.

References

1. Jin, Y.; Li, S.; Kushima, A.; Zheng, X.; Sun, Y.; Xie, J.; Sun, J.; Xue, W.; Zhou, G.; Wu, J.; et al. Self-healing SEI enables full-cell cycling of a silicon-majority anode with a coulombic efficiency exceeding 99.9%. *Energy Environ. Sci.* **2017**, *10*, 580–592. [[CrossRef](#)]
2. Liu, N.; Liu, J.; Jia, D.; Huang, Y.; Luo, J.; Mamat, X.; Yu, Y.; Dong, Y.; Hu, G. Multi-core yolk-shell like mesoporous double carbon-coated silicon nanoparticles as anode materials for lithium-ion batteries. *Energy Storage Mater.* **2019**, *18*, 165–173. [[CrossRef](#)]
3. Xu, Q.; Sun, J.-K.; Yu, Z.-L.; Yin, Y.-X.; Xin, S.; Yu, S.-H.; Guo, Y.-G. SiO_x Encapsulated in Graphene Bubble Film: An Ultrastable Li-Ion Battery Anode. *Adv. Mater.* **2018**, *30*, 1707430. [[CrossRef](#)] [[PubMed](#)]
4. Liang, Y.; Ding, W.; Yao, B.; Zheng, F.; Smirnova, A.; Gu, Z. Mediating Lithium Plating/Stripping by Constructing 3D Au@Cu Pentagonal Pyramid Array. *Batteries* **2023**, *9*, 279. [[CrossRef](#)]
5. Shi, L.; Pang, C.; Chen, S.; Wang, M.; Wang, K.; Tan, Z.; Gao, P.; Ren, J.; Huang, Y.; Peng, H.; et al. Vertical graphene growth on SiO microparticles for stable lithium ion battery anodes. *Nano Lett.* **2017**, *17*, 3681–3687. [[CrossRef](#)] [[PubMed](#)]
6. Yu, H.; Wang, Y.; Jing, Y.; Ma, J.; Du, C.F.; Yan, Q. Surface Modified MXene-Based Nanocomposites for Electrochemical Energy Conversion and Storage. *Small* **2019**, *15*, 1901503. [[CrossRef](#)]
7. Jia, L.; Zou, P.; Gao, X.; Zhao, Y.; He, M.H.; Engelhard, S.D.; Burton, H.; Wang, H.; Ren, X.; Li, Q.; et al. High-performance silicon anodes enabled by nonflammable localized high-concentration electrolytes. *Adv. Energy Mater.* **2019**, *9*, 1900784. [[CrossRef](#)]
8. Yi, R.; Zai, J.; Dai, F.; Gordin, M.L.; Wang, D. Dual conductive network-enabled graphene/ $Si-C$ composite anode with high areal capacity for lithium-ion batteries. *Nano Energy* **2014**, *6*, 211–218. [[CrossRef](#)]
9. Shi, L.; Wang, W.K.; Wang, A.B.; Yuan, K.G.; Jin, Z.Q.; Yang, Y.S. Scalable synthesis of core-shell structured SiO_x /nitrogen-doped carbon composite as a high-performance anode material for lithium-ion batteries. *J. Power Sources* **2016**, *318*, 184–191. [[CrossRef](#)]

10. Guo, J.; Dong, D.; Wang, J.; Liu, D.; Yu, X.; Zheng, Y.; Wen, Z.; Lei, W.; Deng, Y.; Wang, J.; et al. Silicon-based lithium ion battery systems: State-of-the-art from half and full cell viewpoint. *Adv. Funct. Mater.* **2021**, *31*, 2102546. [[CrossRef](#)]
11. Jiao, M.; Wang, Y.; Ye, C.; Wang, C.; Zhang, W.; Liang, C. High-capacity SiO_x (0 ≤ x ≤ 2) as promising anode materials for next-generation lithium-ion batteries. *J. Alloys Compd.* **2020**, *842*, 155774. [[CrossRef](#)]
12. Zhang, K.; Mao, H.; Gu, X.; Song, C.; Yang, J.; Qian, Y. ZIF-Derived Cobalt-Containing N-Doped Carbon-Coated SiO_x Nanoparticles for Superior Lithium Storage. *ACS Appl. Mater. Interfaces* **2020**, *12*, 7206–7211. [[CrossRef](#)] [[PubMed](#)]
13. Feng, K.; Li, M.; Liu, W.; Kashkooli, A.G.; Xiao, X.; Cai, M.; Chen, Z. Silicon-based anodes for lithium-ion batteries: From fundamentals to practical applications. *Small* **2018**, *14*, 1702737. [[CrossRef](#)] [[PubMed](#)]
14. Jeong, H.S.; Kim, J.S.; Jo, K.I.; Choi, J.H.; Koo, J.S. Oriented wrinkle textures of free-standing graphene nanosheets: Application as a high-performance lithium-ion battery anode. *Carbon Lett.* **2021**, *31*, 277–285. [[CrossRef](#)]
15. Park, M.; Lee, D.; Shin, S.; Kim, H.-J.; Hyun, J. Flexible conductive nanocellulose combined with silicon nanoparticles and polyaniline. *Carbohydr. Polym.* **2016**, *140*, 43–50. [[CrossRef](#)] [[PubMed](#)]
16. Ren, W.-F.; Li, J.-T.; Huang, Z.-G.; Deng, L.; Zhou, Y.; Huang, L.; Sun, S.-G. Fabrication of Si Nanoparticles@Conductive Carbon Framework@Polymer Composite as High-Areal-Capacity Anode of Lithium-Ion Batteries. *ChemElectroChem* **2018**, *5*, 3258–3265. [[CrossRef](#)]
17. Choi, S.; Kwon, T.-W.; Coskun, A.; Choi, J.W. Highly elastic binders integrating polyrotaxanes for silicon microparticle anodes in lithium ion batteries. *Science* **2007**, *357*, 279–283. [[CrossRef](#)] [[PubMed](#)]
18. Xin, Y.; Pan, S.; Hu, X.; Miao, C.; Nie, S.; Mou, H.; Xiao, W. Engineering amorphous SnO₂ nanoparticles integrated into porous N-doped carbon matrix as high-performance anode for lithium-ion batteries. *J. Colloid Interface Sci.* **2023**, *639*, 133–144. [[CrossRef](#)]
19. Lee, S.J.; Kim, H.J.; Hwang, T.H.; Choi, S.; Park, S.H.; Deniz, E.; Jung, D.S.; Choi, J.W. Delicate Structural Control of Si-SiO_x-C Composite via High-Speed Spray Pyrolysis for Li-Ion Battery Anodes. *Nano Lett.* **2017**, *17*, 1870–1876. [[CrossRef](#)]
20. Wang, D.; Gao, M.; Pan, H.; Wang, J.; Liu, Y. High performance amorphous-Si@SiO_x/C composite anode materials for Li-ion batteries derived from ball-milling and in situ carbonization. *J. Power Sources* **2014**, *256*, 190–199. [[CrossRef](#)]
21. Umeno, T.; Fukuda, K.; Wang, H.; Dimov, N.; Iwao, T.; Yoshio, M. Novel anode material for lithium-ion batteries: Carbon-coated silicon prepared by thermal vapor decomposition. *Chem. Lett.* **2001**, *30*, 1186–1187. [[CrossRef](#)]
22. Mukhan, O.; Umirov, N.; Lee, B.-M.; Yun, J.-S.; Choi, J.-H.; Kim, S.-S. A Facile Carbon Coating on Mg-Embedded SiO_x Alloy for Fabrication of High-Energy Lithium-Ion Batteries. *Adv. Mater. Interfaces* **2022**, *21*, 2201426. [[CrossRef](#)]
23. Kim, D.S.; Kim, K.H.; Lim, C.H.; Lee, C.; Lee, Y.S. Carbon-coated SiO_x anode materials via PVD and pyrolyzed fuel oil to achieve lithium-ion batteries with high cycling stability. *Carbon Lett.* **2022**, *32*, 321–328. [[CrossRef](#)]
24. Xu, Q.; Sun, J.-K.; Yin, Y.-X.; Guo, Y.-G. Facile Synthesis of Blocky SiO_x/C with Graphite-Like Structure for High-Performance Lithium-Ion Battery Anodes. *Adv. Funct. Mater.* **2018**, *28*, 1705235. [[CrossRef](#)]
25. Zuo, X.; Zhu, J.; Müller-Buschbaum, P.; Cheng, Y.-J. Silicon based lithium-ion battery anodes: A chronicle perspective review. *Nano Energy* **2017**, *31*, 113–143. [[CrossRef](#)]
26. Zhang, M.; Zhang, T.; Ma, Y.; Chen, Y. Latest development of nanostructured Si/C materials for lithium anode studies and applications. *Energy Storage Mater.* **2016**, *4*, 1–14. [[CrossRef](#)]
27. Shaker, M.; Ghazvini, A.A.S.; Qureshi, F.R.; Reza, R. A criterion combined of bulk and surface lithium storage to predict the capacity of porous carbon lithium-ion battery anodes: Lithium-ion battery anode capacity prediction. *Carbon Lett.* **2021**, *31*, 985–990. [[CrossRef](#)]
28. Cao, Y.; Hatchard, T.D.; Dunlap, R.A.; Obrovac, M.N. Mechanofusion-Derived Si-Alloy/Graphite Composite Electrode Materials for Li-Ion Batteries. *J. Mater. Chem. A* **2019**, *7*, 8335–8343. [[CrossRef](#)]
29. Choi, J.-E.; Ko, S.; Jeon, Y.-P. Preparation of petroleum impregnating pitches from pyrolysis fuel oil using two-step heat treatments. *Carbon Lett.* **2019**, *29*, 369–376. [[CrossRef](#)]
30. An, D.; Kim, K.H.; Lim, C.; Lee, Y.-S. Effect of kneading and carbonization temperature on the structure of the carbon block for thermally conductive bulk graphites. *Carbon Lett.* **2021**, *31*, 1357–1364. [[CrossRef](#)]
31. Jo, M.; Sim, S.; Kim, J.; Oh, P.; Son, Y. Micron-Sized SiO_x-Graphite Compound as Anode Materials for Commercializable Lithium-Ion Batteries. *Nanomaterials* **2022**, *12*, 1956. [[CrossRef](#)] [[PubMed](#)]
32. Matthews, M.J.; Pimenta, M.A.; Dresselhaus, G.; Dresselhaus, M.S.; Endo, M. Origin of dispersive effects of the Raman D band in carbon materials. *Phys. Rev. B* **1999**, *59*, R6585. [[CrossRef](#)]
33. Xu, M.; Tan, C. Defect Size Effect and Defect Band Conduction of Ultrathin Oxides After Degradation and Breakdown. *Electron Device Lett.* **2009**, *30*, 410–412.
34. Xia, Y.; Yoshio, M.; Noguchi, H. Improved electrochemical performance of LiFePO₄ by increasing its specific surface area. *Electrochim. Acta* **2006**, *52*, 240–245. [[CrossRef](#)]
35. Wang, Z.Y.; Zhang, H.H.; Zhang, X.Y.; Wang, X.M.; Zhang, X. Yolk-shell porous Fe₃O₄@C anchored on graphene as anode for Li-ion half/full batteries with high rate capability and long cycle life. *Compos. B Eng.* **2022**, *247*, 110308. [[CrossRef](#)]

36. Li, G.; Huang, L.-B.; Yan, M.-Y.; Li, J.-Y.; Jiang, K.-C.; Yin, Y.-X.; Xin, S.; Xu, Q.; Guo, Y.-G. An integral interface with dynamically stable evolution on micron-sized SiO_x particle anode. *Nano Energy* **2020**, *74*, 104890. [[CrossRef](#)]
37. Hernandha, R.F.H.; Rath, P.C.; Umesh, B.; Patra, J.; Huang, C.-Y.; Wu, W.-W.; Dong, Q.-F.; Li, J.; Chang, J.-K. Supercritical CO₂-Assisted SiO_x/Carbon Multi-Layer Coating on Si Anode for Lithium-Ion Batteries. *Adv. Funct. Mater.* **2021**, *31*, 2104135. [[CrossRef](#)]

Disclaimer/Publisher's Note: The statements, opinions and data contained in all publications are solely those of the individual author(s) and contributor(s) and not of MDPI and/or the editor(s). MDPI and/or the editor(s) disclaim responsibility for any injury to people or property resulting from any ideas, methods, instructions or products referred to in the content.